



# Post-Processing of Thresholding or Deep Learning Methods for Enhanced Tissue Segmentation of Whole-Slide Histopathological Images

Michał Marczyk<sup>1,2</sup><sup>a</sup>, Agata Wrobel<sup>3</sup>, Julia Merta<sup>3</sup> and Joanna Polanska<sup>1</sup><sup>b</sup>

<sup>1</sup>Department of Data Science and Engineering, Silesian University of Technology, 44-100 Gliwice, Poland

<sup>2</sup>Yale Cancer Center, Yale School of Medicine, 06511 New Haven, CT, U.S.A.

<sup>3</sup>Faculty of Automatic Control, Electronics and Computer Science, Silesian University of Technology, 44-100 Gliwice, Poland

**Keywords:** Histopathology, Whole-Slide Image, Tissue Staining, Tissue Segmentation, Post-Processing.


**Abstract:** Digital pathology allows for the efficient storage and advanced computational analysis of stained histopathological slides of various tissues. Tissue segmentation is a crucial first step of digital pathology aimed at eliminating background, pen markings, and other artifacts, reducing image size, and increasing the efficiency of further analysis. In most cases, color thresholding or deep learning models are used, but their effectiveness is reduced due to complex artifacts and huge color variations between slides. We propose a post-processing method to increase the tissue segmentation performance of any initial segmentation algorithm. Using a set of 197 manually annotated histopathological images of breast cancer patients and 63 images of endometrial cancer patients, we tested our method with 3 thresholding techniques and 3 deep learning-based algorithms by calculating the Dice index, Jaccard index, precision, and recall. In both datasets, applying post-processing increased precision and recall for thresholding methods and mostly precision for deep learning models. Overall, applying post-processing gave better tissue segmentation performance than initial segmentation methods, significantly increasing Dice and Jaccard indices. Our results proved that thanks to post-processing, the tissue segmentation pipeline is more robust to noises and artifacts commonly present in histopathological images.


## 1 INTRODUCTION

Modern medical imaging enables precise assessment of the stained histopathologic slides of different tissues. The most common staining method is hematoxylin and eosin (HE) since using only these two stains allows the visualization of major tissue structures. Hematoxylin stains nuclei blue, while eosin stains the cytoplasm and connective tissue pink or red. With histopathological slides, pathologists can determine the presence and stage of the disease or the effect of medical treatment (Cooper, L.A., et al., 2018). The development of digital scanners that can obtain high-resolution whole-slide images (WSIs) has contributed to creating extensive datasets with images for various diseases. Digital processing of slides and the decreasing data storage costs stimulated

the development of new algorithms in the fields of image processing and machine learning (Serag, A., et al., 2019). However, the main obstacle is that scanned images are much larger than natural images, so analysis could be extremely time-consuming with high computational capacity requirements.

Most WSIs contain a lot of the background area, which is uninformative for pathologists and only increases the computational cost of image analysis. Tissue segmentation leads to the accurate identification and isolation of relevant regions of WSI, which can significantly impact the efficiency and speed of analysis and decrease the cost of data storage (Salvi, M., et al., 2021). It is also crucial when supervised methods are developed on digital slides since it prevents learning from background noise. Known semi-automated and manual segmentation

<sup>a</sup> <https://orcid.org/0000-0003-2508-5736>

<sup>b</sup> <https://orcid.org/0000-0001-8004-9864>

methods, such as color classification, edge detection, and region growing, can be time-consuming and labor-intensive, especially when dealing with WSIs. Thus in practice one of the two approaches is chosen: traditional thresholding with morphological operations (Alomari, R.S., et al., 2009; Song, Y., et al., 2023) or deep learning-based (DL-based) methods (Riasatian, A., et al., 2020; Lucassen, R.T., et al., 2024). In DL models, an encoder is often used to extract image features while a decoder is used to restore extracted features to the original image size and output the final segmentation results, like in U-Net architecture (Riasatian, A., et al., 2020). SlideSegmenter, based also on convolutional neural network encoder-decoder architecture, introduces some post-processing steps but only for dividing the segmented tissue into cross-sections (Lucassen, R.T., et al., 2024). Additionally, SlideSegmenter provides pen marking segmentation to exclude these regions from tissue segmentation. Even though few techniques have been introduced, there are still many problems unsolved: (i) the requirement for the color of the input image to be normalized, due to differences in staining between laboratories; (ii) manual adjustments of parameters for atypical cases; (iii) the performance of the DL models depends on the datasets used in developing the algorithm or model training; (iv) supervised methods require annotation by an expert pathologist.

Post-processing refinements like hole filling and noise reduction could improve initial segmentation performance. For example, traditional image processing techniques produce initial segmentations that contain single-pixel errors. Also, they might work well on images with high contrast between tissue and background but could struggle with images containing a lot of noise or debris. WSIs often contain artifacts, such as pen markings, air bubbles, and tissue folds, that can interfere with subsequent analyses. Post-processing techniques can be employed to specifically detect and remove these artifacts, resulting in cleaner and more reliable data for downstream tasks. Lastly, DL models also often benefit from post-processing steps that can refine their predictions and improve their accuracy.

Here, we propose a method for post-processing results of various tissue segmentation methods. We tested a combination of our method with three traditional thresholding algorithms and three DL-based solutions on a set of manually annotated HE-stained histopathological images. For thresholding, we chose adaptive methods that are unsupervised, parameter-free, and robust to changes in color intensity distribution between slides.

## 2 MATERIALS AND METHODS

### 2.1 Data

Randomly selected 197 histopathological images of breast cancer patients (BRCA) and 63 images of uterine corpus endometrial cancer patients (UCEC) from The Cancer Genome Atlas (TCGA) obtained through The Cancer Imaging Archive (Clark, K., et al., 2013) were manually annotated by a single expert. The data were saved in .svs format that included slides in different magnifications. For manual annotation, images scanned with a magnification of 2.5x were selected. The annotation was done in a MATLAB environment using the `roipoly()` function or using ImageJ software. All fragments of the tissue in a single slide were marked, excluding artifacts like pen markings, shades, and others, and extremely small fragments.

### 2.2 Adaptive Image Thresholding Methods

Each scanned HE-stained image is composed of three channels, R, G, and B, that represent color components. Thresholding is done on each color separately. Three thresholding methods were tested: (i) GaMRed; (ii) Otsu; and (iii) Peaks. GaMRed is based on the Gaussian mixture decomposition of 1D signal and includes unique data cleaning and post-processing steps (Marczyk, M., et al., 2020). Color intensity from each channel was decomposed into 2 Gaussian components. The component with the higher mean intensity represents background pixels. The threshold value was found as the intersection point between two Gaussians. The Otsu thresholding method (Otsu, N., 1979) was implemented as a two-step algorithm. First, the Otsu method is applied to the original image color channels and cut-off values are found. Second, the Otsu method is applied to image color channels thresholded using cut-off values from the first step, and new cut-off values are estimated. The Peaks method is based on the peak detection algorithm developed for the analysis of 1D mass spectrometry data (Marczyk, M., et al., 2017). The algorithm finds all maxima and minima using the first derivative and then removes small amplitude peaks, similar intensity peaks in close neighborhoods, and the one with too small signal-to-noise ratio. For each color, the threshold value was found as a minimum between the two last peaks of color intensity. All 3 methods allow adaptive estimation of cut-off values for color thresholding without any parameter tuning.

### 2.3 Deep Learning-Based Methods

Three existing methods based on deep learning (DL) models were evaluated for a tissue segmentation task. All models were previously trained by the respective authors on their datasets and used as predictors with TCGA data to mimic real life scenario in which tissue annotations are not provided. All parameters were set as default. The first method, called SlideSegmenter is a convolutional neural network with a post-processing method based on clustering predicted centroid locations of the cross-sections in a 2D histogram (Lucassen, R.T., et al., 2024). Another two methods resulted from the experiments on the U-Net architecture with different network backbones (Riasatian, A., et al., 2020). Based on the published results, the two best backbones were selected for comparison: EfficientNet-B3 and MobileNet.

### 2.4 Post-Processing Methods

The proposed method consists of three subsequent steps: (i) artifacts removal (P1); (ii) region filling (P2); and (iii) small regions removal (P3). Artifacts, which mainly are due to errors during specimen preparation, staining, imaging, or tissue handling, were found and removed using raw WSIs (without thresholding). First, pixels including black and grey color artifacts (resulting from tissue folding, air bubbles, dust, debris and others) were identified using the following steps: (i) create a mask of pixels with a difference between red and green color channels smaller than 10 and a difference between green and blue color channels smaller than 10; (ii) remove the background region resulting from image thresholding from the mask; (iii) remove too small regions from the mask (<30 pixels); (iv) apply morphological closing using a disk of radius 3; (v) apply morphological opening using a disk of radius 3. Pixels including green color artifacts (mostly due to green pen markings) were identified similarly, with modifications only in the first step; the initial mask was created using pixels with a difference between red and blue color channels smaller than 10 and intensity of green color higher than 150. Next, using cleaned images an initial segmentation operation was performed to find the tissue mask using methods described in the previous section. Additionally, pixels with low chroma component (square root of the sum of squared a and b color values resulting from image transformation to LAB color space smaller than 3) were removed from the mask. Next, in P2 holes in the mask were filled using the morphological region filling method with 4 connectivity, and

morphological opening using a disk of radius 3 was applied. Finally, in P3 small area objects were removed from a tissue mask (smaller than 1% of the total tissue mask region). All parameters were estimated on a small pool of HE-stained images scanned with 2.5x magnification, but not used in this manuscript, and then fixed during the analysis. Codes for thresholding and post-processing are available on GitHub under the following address: [github.com/ZAEDPolSI/WSI\\_TissueSeg](https://github.com/ZAEDPolSI/WSI_TissueSeg).

### 2.5 Evaluation Metrics

Four different performance metrics were used to compare tissue segmentation models before and after applying post-processing: Dice coefficient, Jaccard index, pixel precision, and pixel recall. These metrics are defined as follows:

$$Dice = \frac{2 * |Mask \cap GT|}{|Mask| + |GT|} \quad (1)$$

$$Jaccard = \frac{|Mask \cap GT|}{|Mask \cup GT|} \quad (2)$$

$$Precision = \frac{|Mask \cap GT|}{|Mask|} \quad (3)$$

$$Recall = \frac{|Mask \cap GT|}{|GT|} \quad (4)$$

In all equations, *Mask* represents all pixels within the tissue mask, *GT* represents all pixels within manual annotation (ground truth), and  $||$  represents cardinality, which is a sum of pixels in the specified area.

## 3 RESULTS AND DISCUSSION

We created a pipeline for the segmentation of tissue regions on whole slide images, that is composed of two subsequent steps (Figure 1A): (i) initial image segmentation to eliminate the background area of the tissue slide; (ii) image and tissue mask post-processing to refine initial segmentation and isolate only relevant tissue fragments. We tested different methods of thresholding, which estimate the background cut-off values based on the analysis of histograms of color intensities and DL-based models. For the resulting images, we applied image processing techniques used in computer vision which are necessary to increase the quality of the tissue segmentation by removing artifacts, and all other noise components of the image (see example in Figure 1B).

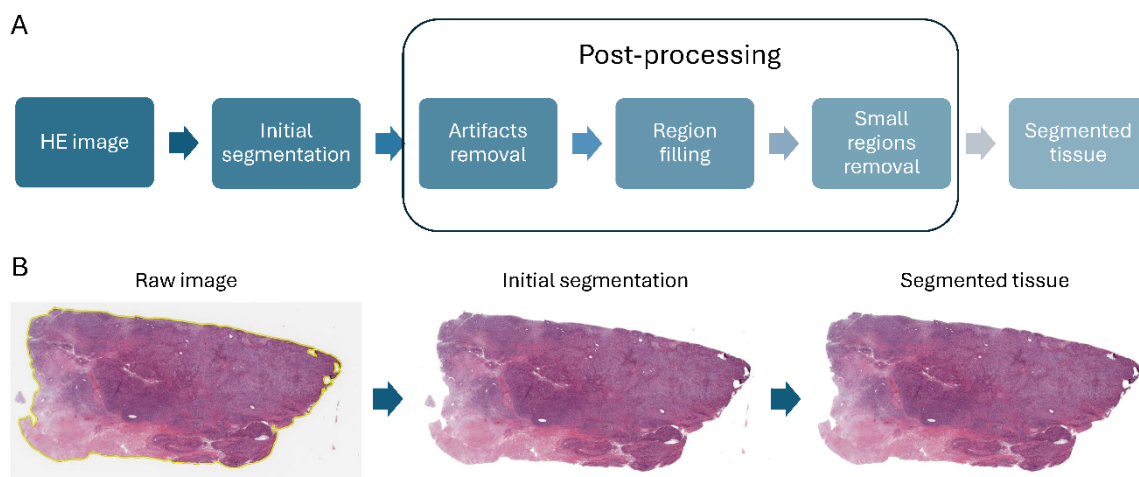


Figure 1: Proposed tissue segmentation algorithm including post-processing step. A) Subsequent steps of the full pipeline. B) Exemplary results of applying the algorithm to the HE image: from raw image (left), through initial tissue segmentation (middle) to segmented tissue after post-processing step (right).

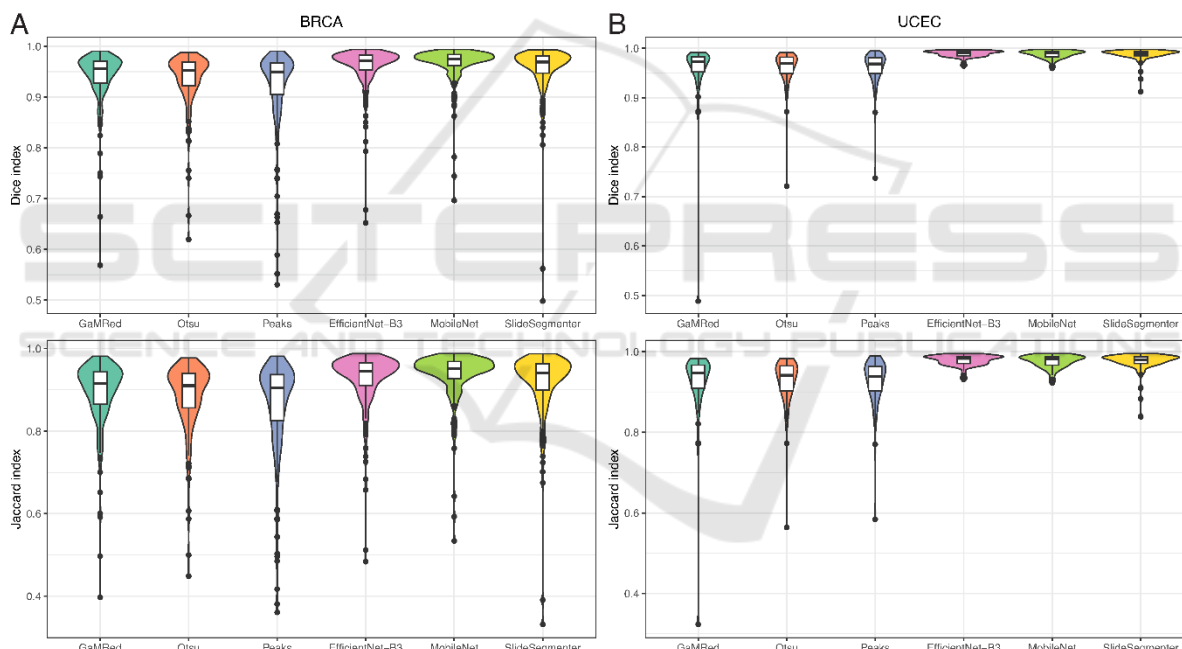


Figure 2: Comparison of tissue segmentation performance between initial segmentation methods (without post-processing) using Dice and Jaccard indices for BRCA (A) and UCEC (B) cohorts.

### 3.1 Initial Segmentation of WSIs

We compared three thresholding methods with three different DL-based methods using Dice and Jaccard indices and precision and recall metrics (Figure 2). Overall, DL-based methods gave better results than traditional methods on both datasets (Table 1).

Among thresholding methods, we observed the highest values for GaMRed (median Dice = 0.9556 in BRCA and 0.9725 in UCEC; median Jaccard =

0.9149 in BRCA and 0.9464 in UCEC) while the lowest for the Peaks method. Among DL-based method, we observed the highest values for MobileNet in BRCA (median Dice = 0.9749; median Jaccard = 0.9511) and EfficientNet-B3 in UCEC (median Dice = 0.9913; median Jaccard = 0.9827). Also, DL-based methods gave higher minimum values of indices than thresholding methods, especially in UCEC (Figure 2B).



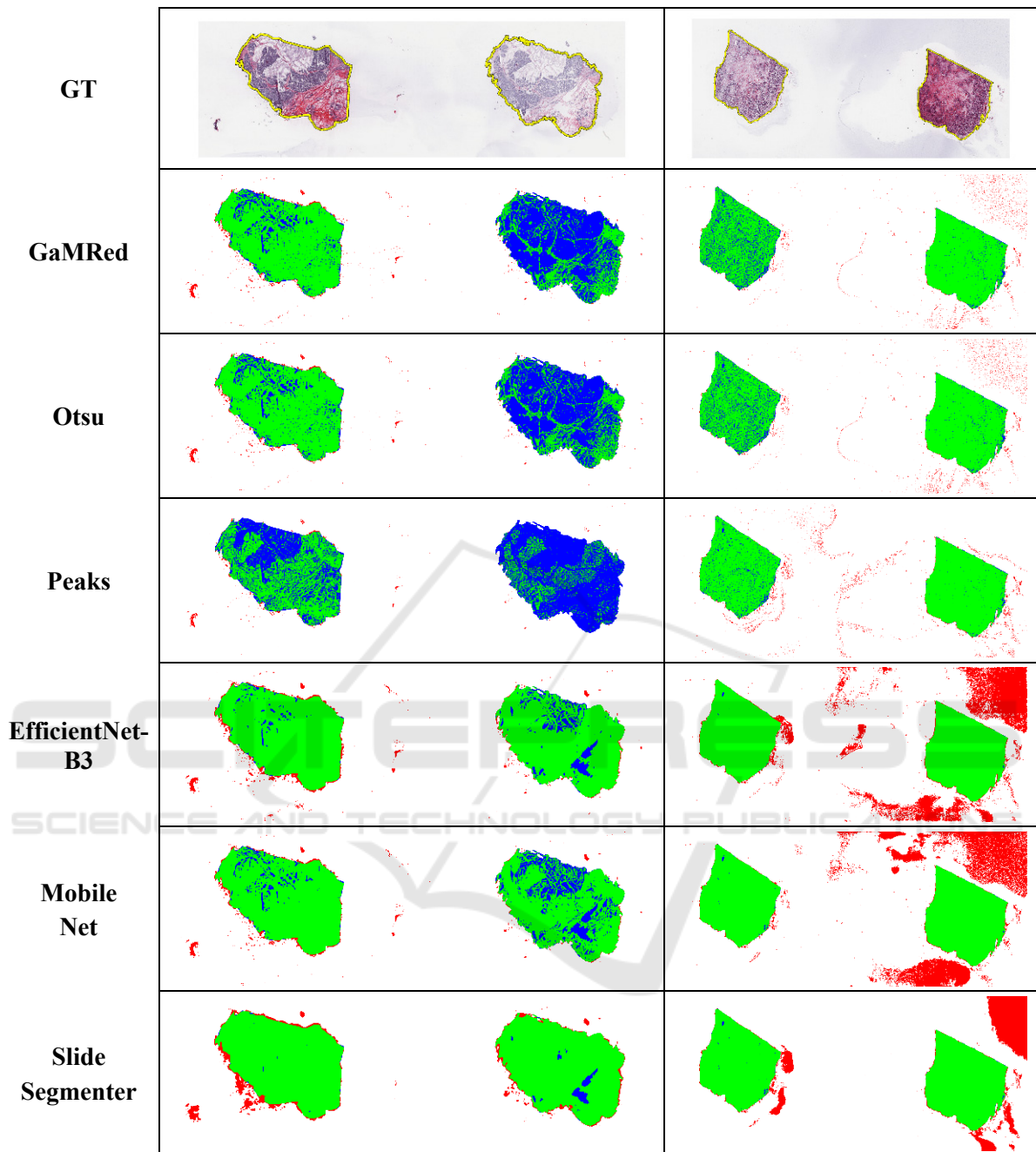


Figure 3: Selected cases with poor initial segmentation (no post-processing). GT is a ground truth segmentation (yellow line around tissue). For each method, the green color indicates true positive, blue false negative, and red false positive regions.

On average, thresholding methods gave higher precision than DL-based methods, but lower recall (Table 1). We found the best precision for Peaks (median = 0.9793 in BRCA and 0.9976 in UCEC) while the worst for SlideSegmenter (median = 0.9461 in BRCA and 0.9933 in UCEC). On the opposite, the best recall was for Slide Segmenter in BRCA (median = 0.9970) and EfficientNet-B3 in UCEC (median =

0.9902). The worst recall was for the Peaks method (median = 0.9193 in BRCA and 0.9437 in UCEC).

In Figure 3, we visualized the worst-case WSI for thresholding methods (left), and DL-based methods (right) in terms of Jaccard and Dice indices. For thresholding methods, we observed mostly false negative regions (colored blue), where the segmentation algorithm omitted tissue regions

selected by the expert giving lower recall. However, in the original images, excluded regions were mostly composed of adipose tissue, which is not relevant in many digital pathology tasks. For the DL-based method, we observed mostly false positive regions (colored red), where the segmentation algorithm marked a larger area than the expert giving lower precision.

A closer investigation of ground truth images shows that areas with noise or artifacts were wrongly selected as tissue regions by DL-based methods, which might bring worse consequences in further analysis.

### 3.2 Influence of Post-Processing on Tissue Segmentation Results

For both datasets and each initial segmentation method, we found a significant increase in almost all performance metrics (p-value from Wilcoxon test smaller than 0.05) after applying the post-processing step (Figure 4 and Tables 1 and 2). Only for EfficientNet-B3 and Slide Segmenter, there was a small decrease in recall in the BRCA dataset (median equal to -0.0001 and -0.0003, respectively).

In terms of Dice and Jaccard indices, a higher gain was observed for thresholding methods than DL-based methods in both datasets, which leads to a similar final performance for all methods (Table 1). Among unsupervised methods, after post-processing, we observed the highest values for GaMRed (median Dice = 0.9865 in BRCA and 0.9941 in UCEC; median Jaccard = 0.9733 in BRCA and 0.9883 in UCEC) while the lowest for the Peaks method. Among DL-based methods, the results are similar giving U-Net-based methods better than Slide Segmenter. Even after post-processing, thresholding methods gave higher precision and lower recall than DL-based methods, but the difference between them is now smaller. Again, we found the best precision for Peaks (median = 0.9923 in BRCA and 0.997 in UCEC) while the worst for Slide Segmenter (median = 0.9657 in BRCA and 0.9964 in UCEC). The best recall was found for Slide Segmenter in BRCA (median = 0.9971) and EfficientNet-B3 in UCEC (median = 0.9976) and the worst for the Peaks method (median = 0.9836 in BRCA and 0.9881 in UCEC).

In Figures 5 and 6, we visualized selected WSI, for which the number of false positive and false negative pixels is significantly reduced after post-processing for each initial segmentation method. The selected image from BRCA (Figure 5) contains a lot of small holes in the tissue, which caused poor segmentation with thresholding methods. The

selected image from UCEC (Figure 6) contains a blue pen marking, that was segmented as tissue mostly for DL-based methods. Also, grey shades below the tissue were falsely marked by Slide Segmenter. All these mistakes were reduced by applying proposed post-processing method.

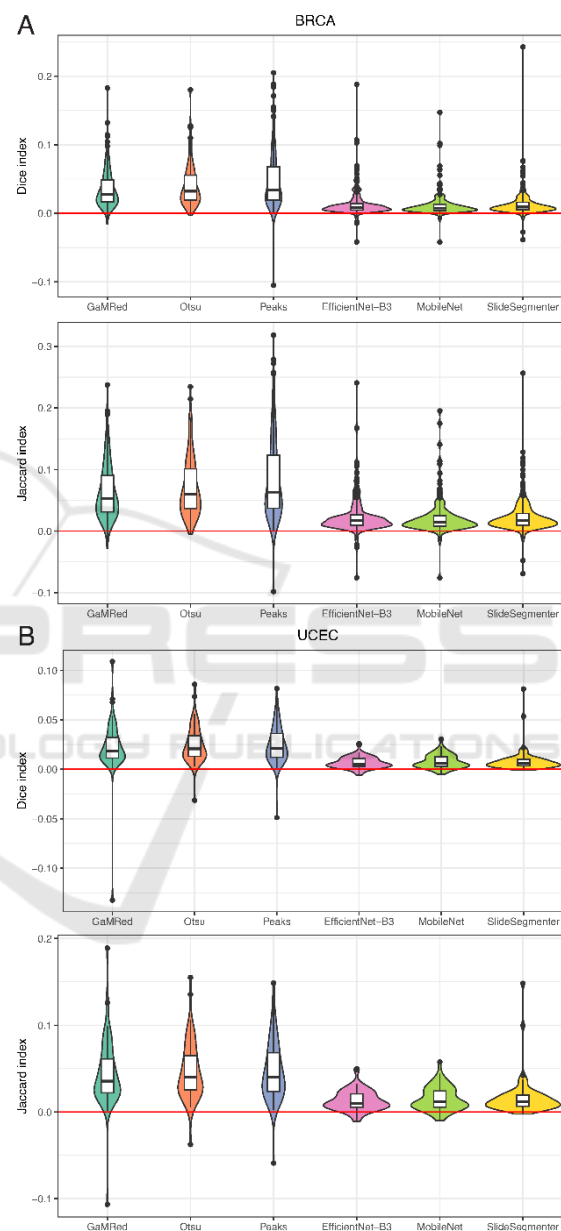


Figure 4: Gain in tissue segmentation performance of different initial segmentation methods after applying post-processing measured using Dice and Jaccard indices for BRCA (A) and UCEC (B) cohorts.

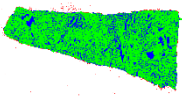
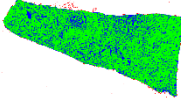
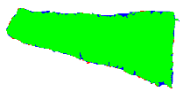
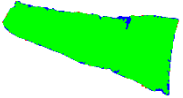
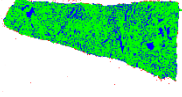
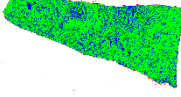

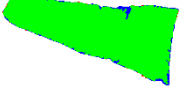
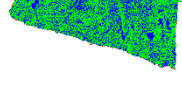
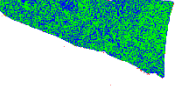
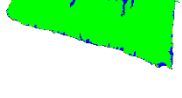
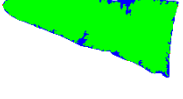


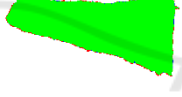

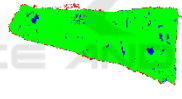
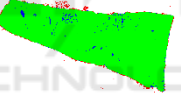

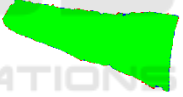

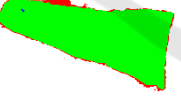


	No post-processing		After post-processing	
<b>GaMRed</b>				
<b>Otsu</b>				
<b>Peaks</b>				
<b>EfficientNet-B3</b>				
<b>MobileNet</b>				
<b>Slide Segmenter</b>				

Figure 5: Selected case from BRCA dataset with high gain in performance after post-processing (right). . For each method, the green color indicates true positive, blue false negative, and red false positive regions.

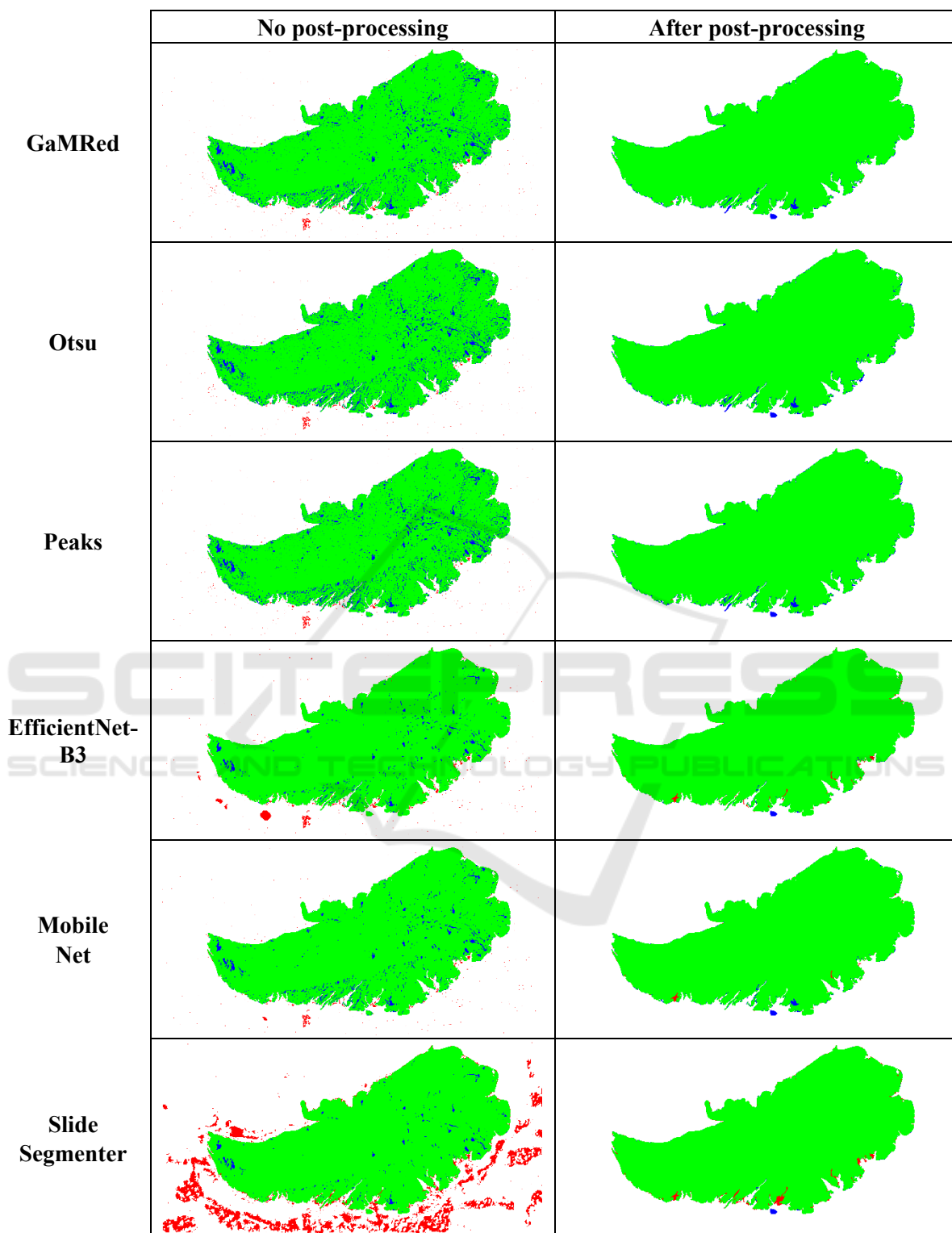


Figure 6: Selected case from UCEC dataset with high gain in performance after post-processing (right). For each method, the green color indicates true positive, blue false negative, and red false positive regions.



Table 1: Median values of performance indices across all images for each dataset and initial segmentation method. Results before and after post-processing are shown. Bold highlights the best value of each index within the dataset and pipeline step.

Dataset	Step	Method	Dice	Jaccard	Precision	Recall
BRCA	Initial segmentation	GaMRed	0.9556	0.9149	0.9736	0.9449
		Otsu	0.9528	0.9099	0.9759	0.9316
		Peaks	0.9498	0.9043	<b>0.9793</b>	0.9193
		EfficientNet-B3	0.9719	0.9454	0.9511	0.9961
		MobileNet	<b>0.9749</b>	<b>0.9511</b>	0.9604	0.9936
		SlideSegmenter	0.9692	0.9403	0.9461	<b>0.9970</b>
	Post-processed	GaMRed	<b>0.9865</b>	<b>0.9733</b>	0.9901	0.9862
		Otsu	0.9859	<b>0.9723</b>	0.9910	0.9848
		Peaks	0.9857	0.9719	<b>0.9923</b>	0.9836
		EfficientNet-B3	0.9833	0.9671	0.9711	0.9965
		MobileNet	0.9856	0.9715	0.9767	0.9955
		SlideSegmenter	0.9798	0.9603	0.9657	<b>0.9971</b>
UCEC	Initial segmentation	GaMRed	0.9725	0.9464	0.9974	0.9487
		Otsu	0.9697	0.9411	0.9974	0.9437
		Peaks	0.9681	0.9382	<b>0.9976</b>	0.9437
		EfficientNet-B3	<b>0.9913</b>	<b>0.9827</b>	0.9935	<b>0.9902</b>
		MobileNet	0.9905	0.9812	0.9950	0.9870
		SlideSegmenter	0.9898	0.9798	0.9933	0.9893
	Post-processed	GaMRed	0.9941	0.9883	<b>0.9997</b>	0.9891
		Otsu	0.9936	0.9872	<b>0.9997</b>	0.9885
		Peaks	0.9938	0.9878	<b>0.9997</b>	0.9881
		EfficientNet-B3	0.9967	0.9935	0.9968	<b>0.9976</b>
		MobileNet	<b>0.9970</b>	<b>0.9940</b>	0.9977	0.9961
		SlideSegmenter	0.9966	0.9932	0.9964	0.9975

Table 2: Gain in performance indices across all images for each dataset and initial segmentation method. Results show the median difference of results after post-processing and initial segmentation. Bold highlights the best value of each index within the dataset.

Dataset	Method	Dice	Jaccard	Precision	Recall
BRCA	GaMRed	0.0281	0.0532	0.0121	0.0389
	Otsu	0.0322	0.0601	0.0105	0.0476
	Peaks	<b>0.0341</b>	<b>0.0632</b>	0.0097	<b>0.0541</b>
	EfficientNet-B3	0.0088	0.0171	0.0158	-0.0001
	MobileNet	0.0076	0.0148	0.0115	0.0006
	SlideSegmenter	0.0091	0.0171	<b>0.0164</b>	-0.0003
UCEC	GaMRed	0.0183	0.0357	0.0022	0.0333
	Otsu	0.0206	0.0400	0.0022	<b>0.0386</b>
	Peaks	<b>0.0209</b>	<b>0.0402</b>	0.0020	0.0385
	EfficientNet-B3	0.0052	0.0102	0.0025	0.0080
	MobileNet	0.0059	0.0117	0.0021	0.0095
	SlideSegmenter	0.0061	0.0121	<b>0.0027</b>	0.0083

### 3.3 Ablation Study

Lastly, we tested the influence of subsequent post-processing methods on the performance of the proposed tissue segmentation pipeline. For each initial segmentation algorithm, we observed similar patterns of changes in the Dice and Jaccard indices (Figure 7). The highest increase was obtained after artifact removal together with region filling (IS+P12; 3% on average), and then a small increase was found

after filtering too small regions (IS+P123) in BRCA, but not in UCEC, where only DL-based methods showed a small increase. Artifact removal alone had the smallest influence on tissue segmentation performance. For DL-based methods, we even observed a small decrease in the Dice index mostly in UCEC. However, we noticed that without this step region filling and small regions removal steps gave much worse results.

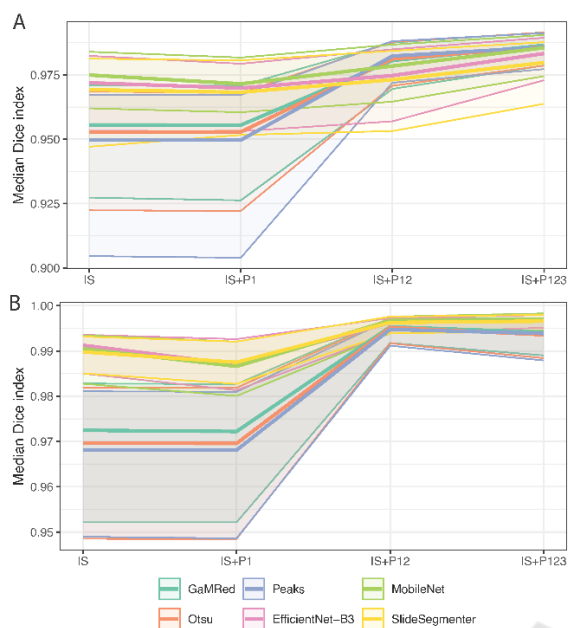


Figure 7: Tissue segmentation results after subsequent steps of the tissue segmentation in BRCA (A) and UCEC (B). IS represents the initial segmentation step, while P123 artifacts removal, region filling, and small regions removal.

## 4 CONCLUSIONS

Segmentation of tissue regions on whole-slide images is an important first step in the advanced computational analysis of stained histopathological slides. We developed a post-processing algorithm that was successfully applied to simple image thresholding methods and more advanced DL-based models. Our analysis proved that the proposed tissue segmentation pipeline is robust to noise and different artifacts observed in the sample, and it can consistently acquire better results than initial segmentation alone. Regardless of a small improvement in performance indices, we visualized some cases to provide visual proof of post-processing necessity. Lastly, all parameters of the proposed method were selected on other, unseen data (but scanned with the same magnification), and fixed during analysis. Thus, there is a potential to improve the results even more through the parameter tuning procedure.

## ACKNOWLEDGMENTS

This publication was supported by the Excellence Initiative - Research University program implemented at the Silesian University of Technology,

grant no. 02/070/SDU/10-21-02 (MM), COMPASS-NMD Project funded by the European Union Horizon Europe program under Grant Agreement 101080874 (JP) and Silesian University of Technology grant no. 02/070/BK\_24/0052 for maintaining and developing research potential.

## REFERENCES

- Cooper, L.A., Demicco, E.G., Saltz, J.H., Powell, R.T., Rao, A., Lazar, A.J.: PanCancer insights from The Cancer Genome Atlas: the pathologist's perspective. *The Journal of pathology* 244, 512-524 (2018)
- Serag, A., Ion-Margineanu, A., Qureshi, H., McMillan, R., Saint Martin, M.-J., Diamond, J., O'Reilly, P., Hamilton, P.: Translational AI and deep learning in diagnostic pathology. *Frontiers in medicine* 6, 185 (2019)
- Salvi, M., Acharya, U.R., Molinari, F., Meiburger, K.M.: The impact of pre-and post-image processing techniques on deep learning frameworks: A comprehensive review for digital pathology image analysis. *Computers in Biology and Medicine* 128, 104129 (2021)
- Alomari, R.S., Allen, R., Sabata, B., Chaudhary, V.: Localization of tissues in high-resolution digital anatomic pathology images. In: *Medical Imaging 2009: Computer-Aided Diagnosis*, pp. 349-358. SPIE
- Song, Y., Cisterino, F., Mekke, J.M., de Borst, G.J., de Kleijn, D.P., Pasterkamp, G., Vink, A., Glastonbury, C.A., van der Laan, S.W., Miller, C.L.: An automatic entropy method to efficiently mask histology whole-slide images. *Scientific Reports* 13, 4321 (2023)
- Riasatian, A., Rasooljafari, M., Babaei, M., Tizhoosh, H.R.: A comparative study of U-net topologies for background removal in histopathology images. In: *2020 International Joint Conference on Neural Networks (IJCNN)*, pp. 1-8. IEEE
- Lucassen, R.T., Blokh, W.A., Veta, M.: Tissue Cross-Section and Pen Marking Segmentation in Whole Slide Images. *arXiv preprint arXiv:2401.13511* (2024)
- Clark, K., Vendt, B., Smith, K., Freymann, J., Kirby, J., Koppel, P., Moore, S., Phillips, S., Maffitt, D., Pringle, M., Tarbox, L., Prior, F.: The Cancer Imaging Archive (TCIA): Maintaining and Operating a Public Information Repository. *Journal of Digital Imaging* 26, 1045-1057 (2013)
- Marczyk, M., Jaksik, R., Polanski, A., Polanska, J.: GaMRed—Adaptive Filtering of High-Throughput Biological Data. *IEEE/ACM Transactions on Computational Biology and Bioinformatics* 17, 149-157 (2020)
- Otsu, N.: A Threshold Selection Method from Gray-Level Histograms. *IEEE Transactions on Systems, Man, and Cybernetics* 9, 62-66 (1979)
- Marczyk, M., Polanska, J., Polanski, A.: Improving peak detection by Gaussian mixture modeling of mass spectral signal. In: *2017 3rd International Conference on Frontiers of Signal Processing (ICFSP)*, pp. 39-43. IEEE